

1 **Detecting gas flares and estimating flaring volumes at** 2 **individual flow stations using MODIS data**

3
4 Obinna C.D Anejionu, G. Alan Blackburn and J. Duncan Whyatt
5 *Lancaster University, Lancaster Environment Centre, United Kingdom;*
6 *Email: o.d.anejionu@lancaster.ac.uk*
7

8 **Abstract**

9 Gas flaring has gained global recognition as a prominent agent of pollution, leading to the estab-
10 lishment of the Global Gas Flaring Reduction (GGFR) initiative, which requires an objective means
11 of monitoring flaring activity. Because auditable information on flaring activity is difficult to obtain
12 there have recently been attempts to detect flares using satellite imagery, typically at global scales.
13 However, to adequately assess the environmental and health impacts of flaring from local to region-
14 al scales, it is important that we have a means of acquiring information on the location of individual
15 active flaring sites and the volume of gas combusted at these sites. In this study we developed an
16 approach to the retrieval of such information using nighttime MODIS thermal imagery. The
17 MODIS flare detection technique (MODET) and the MODIS flare volume estimation technique
18 (MOVET) both exploit the absolute and contextual radiometric response of flare sites. The levels of
19 detection accuracy and estimation error were quantified using independent observations of flare lo-
20 cation and volume. The MODET and MOVET were applied to an archive of MODIS data spanning
21 2000-2014 covering the Niger Delta, Nigeria, a significant global hotspot of flaring activity. The
22 results demonstrate the substantial spatial and temporal variability in gas flaring across the region,
23 between states and between onshore and offshore sites. Thus, while the estimated total volume of
24 gas flared in the region over the study period is large (350 Billion Cubic Metres), the heterogeneity
25 in the flaring indicates that the impacts of such flares will be highly variable in space and time. In
26 this context, the MODET and MOVET offer a consistent and objective means of monitoring flaring

27 activity over an appropriate range of scales and it is now important that their robustness and trans-
28 ferability is tested in other oil-producing regions of the world.

29 **Keywords:** Gas Flare, Thermal Infrared Remote Sensing, MODIS Flare Detection, Niger Delta,
30 Gas Flaring Volume
31

32 **1. Introduction**

33 Gas flaring is one of the processes, alongside venting and reinjection, used to dispose of the
34 natural gas associated with extracted crude oil. Crude oil from a group of wells in an oil field is ini-
35 tially gathered for processing at a flow station where gas is separated from oil. One or a number of
36 flares in the vicinity of the flow station are then used to burn off the gas. Flaring is commonly
37 adopted by oil companies because it is more cost-effective than converting to commercial natural
38 gas. Efforts to empirically assess the environmental impacts of flaring are frequently hampered by
39 limited access to official information on flare locations and volumes, the heterogeneity in spatial
40 and temporal sampling strategies and methods used to collect data and lack of auditability. In order
41 to begin to assess the environmental impacts of flaring in a coherent fashion, there is a pressing
42 need for a robust, consistent and objective means of determining: where active flaring sites are lo-
43 cated; what volume of gas is being flared at each site; and how the distribution and volume of flares
44 has changed over space and time. Consequently, there is a need to develop new methods of acquir-
45 ing such information, and remote sensing seems the most viable option. However, as explained be-
46 low, while there have been several approaches developed for monitoring biomass fires, only a lim-
47 ited number of studies have attempted to map flares or estimate flaring volumes from space. The
48 present study builds upon this work and presents an alternative and enhanced approach.

49 *1.1 Fire detection using satellite imagery*

50 Satellite systems have long been deployed to detect and monitor fires and their effects, due to
51 their timely and repetitive observations, multispectral viewing capabilities, synoptic coverage, and
52 their ability to retrieve information from hazardous locations. Four major classes of algorithm (sin-
53 gle channel threshold, multi-channel threshold, contextual and sub-pixel) have been developed to
54 sense fires from satellite images (Li *et al.*, 2000, Martin *et al.*, 1999). The two main types of signals
55 employed for this purpose are either direct (flames and heat) or indirect (smoke and burned surfac-
56

57 es). Direct signals are most commonly employed in fire detection studies (Movaghati *et al.*, 2009,
58 Justice *et al.*, 2006, Weaver *et al.*, 2004), whilst indirect signals are employed for post fire assess-
59 ment and management (Sedano *et al.*, 2013; Lanorte *et al.*, 2011). Most satellite-based fire detection
60 studies have focused on forest/biomass fires, as their impacts draw considerable attention from the
61 research community and investigations are facilitated by the availability of well-established fire-
62 hotspot algorithms (ATPS, 2013; Wooster *et al.*, 2012; Wang *et al.*, 2012; Xu *et al.*, 2010; Casadio
63 and Arino, 2009; Qian *et al.*, 2009; Roberts and Wooster, 2008; Zhukov *et al.*, 2006; Giglio *et al.*,
64 2003; Prins and Menzel, 1992; Dozier, 1981).

65 Radiation emitted at typical surface fire temperatures mostly lies in the infrared region of the
66 electromagnetic spectrum. Thus, images from sensors such as the Advanced Very High Resolution
67 Radiometer (AVHRR), the Moderate Resolution Imaging Spectroradiometer (MODIS), and the Ge-
68 ostationary Operational Environmental Satellite (GOES) Imager, which have infrared bands, have
69 commonly been used for forest fire detection (Justice *et al.*, 2006; Ichoku *et al.*, 2003; Li *et al.*,
70 2000; Kaufman *et al.*, 1998). These systems have a relatively high temporal resolution, enabling
71 near-continuous monitoring of active fire fronts, which is very important given the ephemeral na-
72 ture of biomass fires.

73 The AVHRR was used to produce the first global fire product and near-real-time global fire
74 data set. The fire detection capability of AVHRR nighttime imagery was first applied on fixed tar-
75 gets of known location (Matson and Dozier, 1981). The level of success achieved in the detection
76 of fixed fire sources led to the use of AVHRR in biomass fire detection. The MODIS sensor has 36
77 spectral bands, some of which are specifically designed for fire monitoring and has improved fire
78 detection capabilities based on existing algorithms developed for AVHRR (Casanova *et al.*, 2005,
79 Justice *et al.*, 2002). However, gas flaring, has not received as much attention as other high temper-
80 ature events (biomass fires, volcanoes, over ground and underground coal fires) and existing fire
81 detection algorithms are often inadequate for detecting gas flares due to the small extent of each
82 flare (Anejionu *et al.*, 2014, Elvidge *et al.*, 2011).

83 *1.2 Detection of gas flares using satellite imagery*

84 Croft (1978) was the first to observe gas flares in nighttime Defence Meteorological Satellite
85 Program (DMSP) and Landsat Multi-spectral Scanner System (MSS) images. While carrying out
86 research to determine blackbody temperatures of sub-pixel fires Matson and Dozier (1981) discov-
87 ered that flares were detectable from nighttime AVHRR imagery. Twelve high temperature indus-
88 trial sources in Detroit (steel mills), and six gas flares in the Persian Gulf were identified using the
89 3.8 μ m and 11 μ m bands of AVHRR. Muirhead and Cracknell (1984) visually inspected daytime
90 AVHRR images and were able to identify gas flares from North Sea oil rigs.

91 Elvidge *et al.* (2007) used DMSP Operational Linescan System (OLS) imagery to visually
92 identify flares, using the circularity and bright centres of lights from flares to aid detection, and this
93 was the first attempt to detect flares on a global scale over extended time periods (1994-2008 inclu-
94 sive). Although the DMSP-OLS method has high temporal resolution (12 hours revisit period), the
95 relatively low spatial resolution (560m – 2.7km) of the imagery limits its ability to accurately detect
96 individual flare sites, particularly amidst urban areas as noted by Elvidge *et al.* (2009a). Further-
97 more, the visual identification technique employed is subjective and time consuming.

98 Casadio *et al.* (2012a) applied an active flame detection algorithm (ALGO3) to nighttime
99 Along Track Scanning Radiometer (ATSR) imagery to detect flares on a global basis. The method
100 is a single band fixed threshold algorithm based on the shortwave infrared band of ATSR (1.6 μ m)
101 and mostly employs temporal persistence of hotspot pixels as an indicator of flaring activity, with
102 the presence of industrial installations (identified from high resolution images available on Google
103 Earth) used to validate the results. However, the method of validation, which does not utilise direct
104 observation of flares on high resolution images, may be inconsistent as not all industrial sites in oil
105 producing regions contain flares. Nevertheless, ALGO3 is more objective than the DMSP-OLS and
106 AVHRR methods, as it adopts a fixed threshold method to automatically discriminate hotspots, thus
107 overcoming the limitations of manual identification. The method has subsequently been revised

108 through the integration of nighttime ATSR and SAR products to detect flares in the North Sea
109 (Casadio *et al.*, 2012b).

110 Whilst the DMSP-OLS and ATSR methods of flare detection can be useful for detecting
111 flares at global level, they are of more limited utility where precise information on flare locations
112 and flare volumes is required for accurate assessment of impacts from local to regional scales. In
113 our previous work, we exploited the higher spatial resolution of Landsat imagery and its extended
114 time-series to detect flares over a period of 29 years (Anejionu *et al.*, 2014). We developed the
115 Landsat Flare Detection Method (LFDM), a multiband threshold technique that used the near infra-
116 red, shortwave infrared and the thermal infrared bands to map active gas flares in the Niger Delta.
117 The LFDM achieved a higher level of spatial accuracy ($\pm 23.85\text{m}$) than earlier methods based on
118 low resolution imagery, and the long archive enabled us to reconstruct the flaring history of the re-
119 gion back to 1984. However, despite the success of the LFDM in flare detection, the low frequency
120 of cloud-free images over the region, lack of nighttime data, and the scan line corrector error in post
121 2003 images limited its potential for estimating flaring volumes.

122 In an attempt to identify alternative data sources that may overcome some of the problems as-
123 sociated with Landsat data, we noted that Elvidge *et al.* (2011) had demonstrated some potential for
124 using MODIS imagery to detect flare sites; this prompted us to investigate this data further. A key
125 advantage of MODIS data is the frequency of acquisition from the Terra and Aqua satellite plat-
126 forms, which increases the likelihood of obtaining cloud-free imagery, which is a critical constraint
127 at the Niger Delta study site and most other regions of the world. Therefore, the present study ex-
128 plores the use of MODIS imagery for accurately and objectively detecting onshore and offshore
129 flares and for estimating flaring volumes.

130

131 *1.2.1 MODIS fire products and gas flare detection*

132

133 The MODIS fire products (MOD14 and MYD14) from Terra and Aqua platforms, respective-
134 ly, were developed for the identification and monitoring of wild fires. The fire detection algorithms

135 are based on those developed for AVHRR, but with new capabilities (previous AVHRR 3.75 μ m
136 waveband was shifted to 3.95 μ m in MODIS, to minimise the effects of atmospheric water vapour
137 absorption and reflected solar radiation by 40% (Kaufman *et al.*, 1998)). Fire pixels are retrieved
138 using a hybrid of absolute and contextual processes that involve the application of sets of thresholds
139 on bands 22 (3.95 μ m), 31(11 μ m) and 16 (0.86 μ m) (Giglio *et al.*, 2003; Justice *et al.*, 2002).

140 However, as observed by Elvidge *et al.*, (2011), the MODIS fire product is less efficient at de-
141 tecting gas flares because thresholds in the algorithms were adapted to minimise the detections of
142 small fires such as gas flares and to maximise the detection of larger and more intense biomass fires
143 (Kaufman *et al.*, 1998, Justice *et al.*, 2002, Giglio *et al.*, 2003). In addition, the algorithms only de-
144 tect fires on landmasses (onshore) as they are not expected to occur on water bodies (offshore). This
145 is a significant constraint of the product in the present context because a considerable proportion of
146 flaring activities in the Niger Delta are located offshore. However, ongoing improvements of the
147 MODIS fire product (collection 6) are expected to revise the water mask to facilitate offshore gas
148 flare detection (Giglio *et al.*, 2014; Csiszar *et al.*, 2012). Exploratory investigations (Elvidge *et al.*,
149 2011) revealed that the MODIS fire products were conservative in flare detection, compared with
150 visual observations directly made from the MODIS band 22 image. This indicates that a bespoke
151 algorithm is required for the detection of gas flares from MODIS imagery.

152

153 1.2.2 Flare volume estimation from satellite imagery

154 The first attempt to estimate the volume of gas flared using satellite imagery was conducted
155 by Elvidge *et al.* (2007), who used nighttime DMSP-OLS imagery to quantify the changes in total
156 annual flaring volume for each of the world's oil producing countries over the period 1995 – 2006.
157 The technique was further improved and the period of study extended to 15 years (1994 – 2008) by
158 Elvidge *et al.* (2009a). However, the researchers noted some limitations in the DMSP-OLS tech-
159 nique such as the saturation of the DMSP-OLS visible band due to the brightness of gas flares, as
160 well as the inability of the technique to detect flares in the mid-to-high latitudes in the summer time

161 due to solar contamination. In addition, the lack of onboard calibration of the DMSP-OLS visible
162 band limits the ability to estimate the total radiative output from flares, and the intercalibration of
163 different DMSP-OLS sensors was based on the assumption that electrically generated lights around
164 Sicily, Italy, had remained constant over the period of study (1994-2008) which was not validated.
165 Furthermore, Elvidge *et al.* (2011) found it very difficult to discriminate flares in lit urban areas and
166 lights from oil facilities other than gas flares are often included in DMSP-OLS signals. These limi-
167 tations will each contribute to uncertainties in estimates of flaring volume using the DMSP-OLS
168 and suggest that there is value in exploring the potential of alternative remote sensing systems.

169 The first attempt to estimate flaring volume from MODIS was made by Gallegos *et al.*
170 (2007). They found that the reference flare sites with known gas flaring volumes were in some cas-
171 es not detectable with the MODIS data, and therefore concluded that MODIS data would only be
172 marginally useful in estimating daily gas flaring volumes. However, as noted by Elvidge *et al.*,
173 (2011) the researchers did not work with enough MODIS images to test its capability for monthly or
174 annual estimation of gas flaring volumes.

175 Elvidge *et al.* (2011) found that the MODIS fire product (MOD14) was inefficient at esti-
176 mating flaring volumes. In many countries such as Nigeria, estimates were typically 25% lower
177 than estimates derived from DMSP-OLS imagery due to the undersampling of gas flares by
178 MOD14. Furthermore, for countries in the Amazon such as Bolivia, where biomass fires are com-
179 mon, the volume estimates exceeded those derived from DMSP-OLS due to the erroneous inclusion
180 of other fire sources. However, Elvidge *et al.* (2011) did find a close correspondence between flare
181 volumes estimates made directly from the difference between MODIS bands 22 and 31, and the re-
182 sults previously obtained from DMSP-OLS for a particular sample year (but as noted previously
183 there are several limitations with the DMSP-OLS technique itself). Therefore, based on this finding,
184 they recommended further exploration of MODIS for flare detection and volume estimation.

185
186 In this study, we set out to achieve the following objectives:

- 187 i. develop a technique to detect active gas flare sites from MODIS imagery,
- 188 ii. develop a technique to estimate the volume of gas flared from individual flare sites
189 from MODIS imagery,
- 190 iii. apply these techniques to the MODIS archive in order to quantify the trajectories of
191 gas flaring activity and flaring volumes in a globally significant gas flaring region.

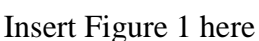
192

193 **2. Study Area**

194

195 The Niger Delta (Figure 1) is a densely populated region with over 10 million people and covers an
196 area of approximately 70,000km² (NPC, 2010). It is the largest source of hydrocarbons in Nigeria
197 (Tuttle *et al.*, 1999) and the region has been greatly impacted by ongoing oil and gas exploration
198 and extraction, which commenced in 1958. Importantly, the Niger Delta is home to the third largest
199 mangrove forest in the world with rich biodiversity (Niger Delta Awareness, 2007). Consequently
200 the Niger Delta is ranked as one of the highest conservation priorities in West Africa (IUCN, 1994)
201 as it provides the natural habitat for a wide variety of endemic coastal and estuarine fauna and flora,
202 supporting over 60% of the total species in Nigeria (World Bank, 1995, cited in Ugochukwu 2008;
203 IUCN, 1994). Despite its importance, the region is virtually unprotected and as a result has been the
204 focus of increasing research activity in recent years, particularly on the impacts of oil exploitation
205 on the environmental (Bayode *et al.*, 2011; Nwaogu and Onyeze, 2010; Eregha and Irugh, 2009),
206 socio-cultural and economic characteristics of the region (Aghalino and Odeh, 2010; Ajiboye *et al.*,
207 2009). Among the many activities associated with the oil industry that directly affect the environ-
208 ment, such as oil spillage and fires, deforestation, dredging and associated waste, gas flaring is a
209 prominent agent of pollution in the region (Ovri and Iroh, 2013; Ovuakporaye *et al.*, 2012; Abdul-
210 kareem *et al.*, 2012; Dung *et al.*, 2008). However, efforts to empirically assess the environmental
211 impacts of flaring in the Niger Delta have been hampered by limited access to official information
212 on flare locations and volumes and difficulties in undertaking field investigations due to security
213 issues. Thus, previous research has mostly been speculative or restricted to small areas surrounding

214 individual flares (Obia *et al.*, 2011; Abdulkareem, *et al.*, 2012; Anomohanran, 2012; Oseji, 2011;
215 Odjugo and Osemwenkhae, 2009; Dung *et al.*, 2008). Hence, there is an important need to develop
216 a comprehensive understanding of flaring activity and its impacts in the Niger Delta, particularly
217 given that Nigeria ranks second among gas flaring countries globally (Elvidge *et al.*, 2009).

218  Insert Figure 1 here

219 **3. Methods**

220 **3.1 Data and preprocessing**

221 Day and nighttime MODIS images from the Terra and Aqua platforms were acquired from
222 the NASA's Earth Observing System Data and Information System (EOSDIS)
223 (<http://earthdata.nasa.gov/>). Having explored the data available for all months of the year, it was
224 found that only data for the months of December and January had acceptable levels of cloud-free
225 coverage as all images in all other months had greater than 50% cloud coverage. These months fall
226 within the Harmattan weather period, with drier and less humid conditions experienced in the Niger
227 Delta. This study consequently used MODIS data from these months for the period 2000 to 2014. In
228 total, 1643 MODIS images (899 Terra and 744 Aqua) were obtained and processed for the study.
229 Individual images with greater than 30% cloud cover were removed, leaving a total of 588 images
230 for further analysis. The MODIS raw DN values were processed with the ENVI MODIS toolkit to
231 derive spectral radiances. All images were georeferenced to the WGS 1984 coordinate system then
232 clipped to the study area. Bi-monthly temporal composites were computed from the data obtained in
233 the adjacent months of December and January using a maximum value compositing technique that
234 selected the maximum radiance from each pixel from all the images in the bi-monthly stack (Stoms
235 *et al.*, 1997). This approach records the radiance value for each pixel which is least attenuated by
236 cloud cover and therefore effectively generates a cloud-free composite image and minimises noise
237 due to other atmospheric constituents (Jonsson and Eklundh, 2004). In the absence of data on at-
238 mospheric conditions over the study sites on the various image acquisition dates, the compositing

239 technique provided a practical and effective atmospheric correction method as has been well estab-
240 lished and previously applied to MODIS data (Hueté *et al.*, 2002; Holben, 1986). This procedure
241 generated 15 temporal composite images of the study site covering the 2000-2014 period at an ap-
242 proximately annual sampling interval.

243

244 3.1.1 Examination of the flare detection potential of MODIS bands

245 Each MODIS band was examined interactively and compared to reference data of known flare
246 locations (see section 3.2.1 below) in order to determine its suitability for flare detection. Only a
247 small number of bands showed any capabilities for flare detection (Figure 2, see Table 1 for band
248 characteristics). The daytime shortwave infrared (band 6, 1.64 μm ; band 7, 2.11 μm) showed some
249 potential for flare detection, as in previous research with Landsat data (Anejionu *et al.*, 2014). In-
250 deed, Elvidge *et al.* (2013) found that for gas flares (at 1800K) the peak radiant emission is in the
251 shortwave infrared at around 1.6 μm . However, in the present study the daytime shortwave infrared
252 bands were highly sensitive to other reflective materials including clouds, the built-environment and
253 sands in and around rivers. Similar confounding effects have been found when attempting to use
254 daytime shortwave infrared VIIRS data (band M10, 1.6 μm) for flare detection (Elvidge *et al.*,
255 2013). Furthermore, gas flares could not be detected from nighttime MODIS bands 6 and 7 as the
256 MODIS reflective bands are turned off during “night mode” scans (MODIS Characterization Sup-
257 port Team, 2012). From the MODIS thermal bands that have previously been used in biomass fire
258 detection only bands 21 and 22 (both 3.96 μm) were useful for flare detection, while band 31 (11.02
259 μm) had no value for flare detection whether acquired during daytime or nighttime. Daytime band
260 21 and 22 data were responsive to flares but were also sensitive to other hot and reflective surfaces
261 such as urban areas, bare lands and sands due to solar irradiation. Nighttime data were equally re-
262 sponsive to flares but were not subjected to the solar-induced confounding effects. While bands 21
263 and 22 had similar responses to gas flares, band 21 is known to be noisier with higher quantization
264 error than band 22 (Giglio *et al.*, 2003) and this was evident in the data used for the present study.

265 The noisiness of band 21 is due to the fact that it has a relatively higher dynamic range than band 22,
 266 to avoid saturation over very hot and large targets and this has made it useful for the detection of
 267 biomass fires and volcanoes. However, due to the relatively smaller size of gas flares band 22 is
 268 more appropriate. Based on the spectral emission patterns of gas flares elucidated by Elvidge *et al.*
 269 (2013) flares at 1800K have a peak radiant emission at around 1.6 μm therefore MODIS band 22
 270 (3.96 μm) is on the trailing edge of flare emissions. Using Plank's and Stefan-Boltzmann's Laws,
 271 we estimated that for flares at 1800K MODIS band 22 would sample approximately 0.63% of total
 272 radiant output, whereas for flares at 1250K band 22 would sample 1.01% of the radiant output.
 273 Therefore, MODIS band 22 would become relatively more effective as flare temperature decreases
 274 but would be less suitable than a shortwave infrared band for higher temperature flares. However
 275 for the practical reasons given above related to solar effects and nighttime MODIS scan configura-
 276 tion, nighttime band 22 data was used for the development of the flare detection and volume estima-
 277 tion techniques described in this study.

278 Insert Figure 2 Here
 279
 280
 281

Table 1. Spectral and spatial characteristics of the MODIS bands examined in this study.

Band	Bandpass (μm)	Spatial Resolution (m)
6	1.628-1.652	500m
7	2.105-2.155	500m
21	3.929-3.989	1000m
22	3.929-3.989	1000m
31	10.780-11.280	1000m

282
 283
 284
 285

286 **3.2 Development of the MODIS Flare Detection Technique (MODET)**

287 A method which utilised the radiometric and spatial properties of gas flares was chosen for
 288 detecting flares and discriminating them from other features with high thermal emissions. Gas flares
 289 are smaller in size than biomass fires, occur at flare stacks and pits permanently fixed to a particular
 290 location and are mostly continuously active (SPDC, 2013; Elvidge *et al.*, 2011; Friends of the Earth,

291 2005). The continuous combustion of gas is expected to generate a considerable thermal signal that
292 would distinguish fire from non-burning background features. However, given the varying envi-
293 ronmental context of flares in the Niger Delta (ranging from offshore, to mangrove swamp and to
294 rainforest areas), we found that a simple threshold method alone was unsuitable for flare detection.
295 We therefore fused a traditional radiometric threshold algorithm with a spatial filtering algorithm
296 capable of identifying gas flares based on differences in radiation between the flare pixels and sur-
297 rounding pixels. This combination of radiometric and spatial filtering algorithms has been found to
298 be valuable when using thermal imagery for fire detection (Roberts *et al.*, 2005; Roberts and
299 Wooster, 2008). In the present study, the radiometric algorithm applied a threshold to band 22 to
300 identify potential flare sites (see section 3.2.2 below which discusses the selection of the threshold
301 value). The spatial filtering algorithm is an adaptation of earlier methods used in the identification
302 of active fires (Flasse and Ceccato, 1996; Prins and Menzel, 1992) and flares from MODIS imagery
303 (Elvidge *et al.*, 2011). A high pass filter was applied to band 22 in order to identify areas of sharp
304 spatial change in radiance. A 3x3 kernel was found to be most suitable for highlighting differences
305 between flares and immediate surrounding pixels. The results of the high pass filtering were subse-
306 quently reclassified using a threshold to identify potential flare pixels (section 3.2.2 discusses the
307 threshold value). The results of the spatial filtering were then overlaid with the results from the ra-
308 diometric threshold and potential flare pixels common to both algorithms were taken to be the ac-
309 tive flare pixels. The key stages of the MODET are summarised in Figure 3.

310 Given the spatial resolution of the MODIS imagery (1km) it is feasible that within a single
311 pixel or group of pixels identified as flares there may be one or more active flares associated with a
312 flow station. Flares associated with a flow station are typically located within a radius of several
313 hundred metres whereas individual flow stations are located at least several tens of kilometres apart.
314 Therefore, rather than identifying flares (from individual stacks/pits), the MODET actually detects
315 the flaring activity associated with individual flow stations, which we refer to as ‘flare sites’.

316 Insert Figure 3 here

317

318 *3.2.1 Reference dataset and validation method*

319 High resolution images covering the Niger Delta obtained from Google Earth were visually
320 inspected in order to construct a reference dataset of active flare sites. This approach was adopted as
321 a ground-based survey of flare locations was not feasible at the time of research, due to logistical
322 and security issues associated with fieldwork in the region. Visible fires from gas flares (e.g. centre
323 of Figure 4) were used in conjunction with clearly discernible physical structures such as buildings,
324 pipelines, flare pits and flare stacks to confirm the locations of active flare sites. This method for
325 collecting reference data on flare locations has been employed effectively by previous researchers
326 (Anejionu *et al.*, 2014; Casadio *et al.*, 2012; Elvidge *et al.*, 2009b). The high resolution data cover-
327 ing the study area comprise a mosaic of images acquired over different time periods; as a result no
328 single image or acquisition date was able to provide enough reference flare sites for validation.
329 Hence, the reference dataset of 43 active flare sites was obtained from a range of high resolution
330 images acquired between 2002 and 2007 and this was compared to the outputs of the MODET ap-
331 plied to MODIS imagery for the corresponding years. All active flare sites within the boundaries of
332 the high resolution images were identified by placing a 1km resolution vector grid over the imagery
333 and systematically viewing and identifying all flare sites within each grid cell. The boundaries of
334 the high resolution images were used to define the sample areas for validating the MODET, there-
335 fore errors of omission and commission could be quantified and the user and producer accuracies
336 for detection computed.

337

Insert Figure 4 here

338

339 *3.2.2. Identification of optimal thresholds and assessment of detection and spatial accuracy*

340 To identify the optimal thresholds for the radiometric and spatial filtering algorithms, a range
341 of radiance values were tested. Characteristic background radiance of onshore and offshore envi-
342 ronments for the original and spatially filtered band 22 images were used to identify suitable ranges

343 of thresholds for testing. In turn, thresholds of between 0.5 and 0.7 $\text{Wm}^{-2} \text{sr}^{-1} \mu\text{m}^{-1}$ (with an incre-
 344 ment of 0.01) were tested for the radiometric algorithm and between 0.2 and 0.5 $\text{Wm}^{-2} \text{sr}^{-1} \mu\text{m}^{-1}$ (in-
 345 crement 0.1) for the spatial filtering algorithm, and the accuracy of the outputs determined using the
 346 validation approach outlined above. Table 2 shows the accuracy statistics for a selection of the best
 347 performing combinations of threshold values. The combination of thresholds for the radiometric
 348 and spatial algorithms which maximised both user's and producer's accuracy (combination H in
 349 Table 1) was selected for the MODET (Figure 3).

350 **Table 2.** Summary statistics of accuracies computed from the different threshold combinations based on a reference
 351 data set of 43 known flares.

Combina- tion	Radiometric Threshold ($\text{Wm}^{-2} \text{sr}^{-1} \mu\text{m}^{-1}$)	Spatial Threshold ($\text{Wm}^{-2} \text{sr}^{-1} \mu\text{m}^{-1}$)	Total Detections	Flares omitted	Detections Confirmed	Producer's accuracy	User's Accuracy
A	0.66	0.4	35	10	35	76.7	100.0
B	0.645	0.4	35	10	35	76.7	100.0
C	0.6	0.4	36	9	36	79.1	100.0
D	0.56	0.4	40	6	40	86.1	100.0
E	0.6	0.2	43	4	41	90.7	95.4
F	0.6	0.3	42	5	41	88.4	97.6
G	0.6	0.5	40	6	40	86.1	100.0
H	0.56	0.3	43	4	43	90.7	100.0

352
353

354 To compute the spatial accuracy of the MODET, the coordinates of the centroids of 20 flare
 355 sites detected by the technique were compared with the coordinates of corresponding reference
 356 flares derived from the high resolution imagery (Table 3). Offsets in latitude and longitude between
 357 the MODET detection and the reference flare locations were used to compute the root mean square
 358 error (RMSE) for each flare site and the mean RMSE (844m) was used as a measure of the spatial
 359 accuracy of the MODET.

360 **Table 3.** Details of the MODET detections and reference flare locations used to compute the spatial
 361 accuracy of the MODET
 362

MODET Detections			Reference flares		
Long (°)	Lat (°)	Flare Site ID	Long (°)	Lat (°)	RMSE (m)
6.521486	5.659878	MODET 11	6.517196	5.659283	480
6.708013	5.456133	MODET 22	6.694344	5.458499	1539
6.662598	5.387761	MODET 27	6.657883	5.386097	555

6.616185	5.239537	MODET 31	6.628775	5.236312	1442
6.493413	5.191626	MODET 33	6.491294	5.197543	697
6.506888	5.097302	MODET 35	6.506823	5.099702	266
6.364653	5.026933	MODET 37	6.358577	5.024974	708
6.379626	4.882203	MODET 47	6.372342	4.885274	877
6.08198	4.657122	MODET 53	6.07764	4.661282	667
7.06385	4.652631	MODET 55	7.060293	4.652185	397
6.272682	4.628248	MODET 56	6.26458	4.628168	899
6.673079	4.544832	MODET 60	6.664416	4.549694	1102
7.009052	4.552018	MODET 61	7.003554	4.55646	784
8.016076	4.547077	MODET 62	8.010454	4.552057	833
7.049092	4.544832	MODET 63	7.045435	4.553114	1004
6.634151	4.523871	MODET 64	6.632621	4.526412	329
5.280867	5.668245	MODET 123	5.275077	5.673164	843
6.718174	4.554332	MODET 148	6.710037	4.55965	1078
5.133817	5.84871	MODET 238	5.133365	5.860184	1274
5.17438	5.614197	MODET 173	5.173002	5.624002	1099

Note: Mean RMSE = 844m

363

364

365 3.2.3 Application of the MODET

366

367

368

369

370

371

372

373

374

375

376

377

378

379

The MODET was subsequently applied to the bi-monthly (December-January) temporal composites covering the 2000 to 2014 study period. The number of times each flare site was detected was recorded with sites that were detected only once over the fifteen sampling occasions removed as false detections. This is because once flow stations are constructed and flares become active they burn continuously over their operational period which is typically in decadal time scale (SPDC, 2013, Onwuka, 2003). Therefore gas flares are highly unlikely to occur on only a single sampling occasion, whereas biomass fires, or other high radiance features are much more ephemeral. Previous studies have utilised a similar persistence approach in discriminating flares from false identifications (Casadio *et al.* 2012a, 2012b) or to normalise the impact of background noise on flare detections (Elvidge *et al.*, 2009a). Since we do not have data from subsequent years to confirm if the flares detected in 2013/14 were persistent, we incorporated them into the output, on the basis that their detections satisfied the MODET procedure. The flares identified within the study period were used to obtain a flaring history detailing the spatial and temporal variations in the distribution of active flares in the region. The Nigerian political map was used to allocate the detected flares to the

380 different states in the region. As the map did not delineate offshore state boundaries, offshore flares
381 were objectively allocated to the state with the nearest onshore boundary by Euclidean distance.
382 The onshore and offshore flaring was then used to calculate the overall activity for each state, on
383 each sampling occasion.

384

385 ***3.3 Development of the MODIS Flare Volume Estimation Technique (MOVET)***

386 The MOVET is based on the concept that the volume of gas flared at each flow station for any
387 given time period (i.e. the combustion rate) would determine the intensity of fire at that location,
388 and by extension the magnitude of the spectral radiance emitted at the location, captured by the
389 MODIS sensor. We therefore set out to establish a method that would optimally harness the infor-
390 mation contained in the radiance at the flare sites (flare pixels) and surrounding environment (back-
391 ground pixels), to estimate the volume of gas flared. Having identified the locations of flare sites
392 using the MODET, MODIS band 22 was analysed further to derive a statistical relationship be-
393 tween the spectral radiance of flare sites and the volume of gas flared. Due to the difficulty in ac-
394 cessing official records of oil and gas related information in Nigeria (which gave rise to the present
395 research on alternative information sources on flaring), it was only possible to match detections
396 from the MODET with records of the volume of gas flared at 29 sample flow stations across the re-
397 gion in December 2004 (data sourced from Nigerian National Petroleum Corporation). Consequent-
398 ly, the band 22 temporal composite image from December 2004 was used together with the flare
399 volume records in order to develop the MOVET.

400 A number of different approaches were explored in order to develop the MOVET. The first
401 stage was to apply a series of different methods for extracting pixel values from the vicinity of de-
402 tected flare sites, and the second was to use a number of different ways to derive radiometric varia-
403 bles from the extracted pixels. The combination of extraction approach and radiometric variables
404 that produced the strongest correlation with the flare volume records was used for the MOVET. The
405 pixel extraction approaches that were tested were: (i) use of individual or groups of flare pixels at

406 each flare site; (ii) identification of a centroid location for individual or groups of flare pixels at
407 each flare site then construction of a circle of different sizes (1, 2, 3km) around this point and ex-
408 traction of all pixels which intersected with the circle (to incorporate flare and background pixels);
409 (iii) use of a buffer of 1 to 3 pixels around each individual or group of flare pixels and extraction of
410 all flare and background pixels within this region. The radiometric variables derived from the
411 groups of pixels extracted in the previous stage were: (i) statistical parameters (minimum, maxi-
412 mum, range, sum, mean and standard deviation); (ii) combinations of the statistical parameters such
413 as the product of mean and maximum, standard deviation and sum, and the difference between the
414 maximum and minimum. These combinations of statistical parameters enabled quantification of
415 various relationships between flare and background radiance values, for example, the difference be-
416 tween the maximum and minimum measured the radiance increase above background generated by
417 flares; (iii) calculation of the Fire Radiative Power based on fire and background pixel radiances
418 (Wooster *et al.*, 2003); (iv) calculation of the magnitude of slope in radiance between flare pixels
419 and background pixels expressed as a mean value for each group of pixels considered. The optimal
420 combination of pixel extraction approach and radiometric variables was used as the basis as
421 MOVET as follows.

422 The MOVET is based on the combined use of the total radiation intensity at the flare site and
423 a measure of the localised influence of the flares over their surrounding environment. It is thus a
424 hybrid absolute and contextual approach for estimating flare volume which incorporates radiance
425 values of flare pixels and surrounding pixels. A buffer of 1 pixel around flare pixels (i.e. in the case
426 of an individual flare pixel constitutes a 3x3 pixel window with the flare at the centre) was found to
427 be optimal for capturing the radiometric zone of influence of flares and some areas of background
428 that were unaffected by flares. The 1 pixel buffer accommodated the variability and effects of gas
429 flares in the different environmental contexts. Regression analyses performed on reported flare vol-
430 ume and radiance statistics for the 29 sample flare sites demonstrated that the optimal predictor of

431 flare volume was a combination of the sum and standard deviation of radiance values of the extract-
432 ed pixels at flare sites ($R^2 = 0.77$, $p < 0.01$; see Figure 5) which was used as the basis of the MOVET:

$$433 \quad V = 375(\Sigma r^2 \cdot \sigma r) + 6230 \quad (1)$$

434 where V = flare volume (Million Cubic Metres);

435 Σr = sum of radiance ($\text{Wm}^{-2} \text{sr}^{-1} \mu\text{m}^{-1}$);

436 σr = standard deviation of radiance ($\text{Wm}^{-2} \text{sr}^{-1} \mu\text{m}^{-1}$).

437 Here Σr^2 quantifies the absolute intensity of emissions of the flare site while σr provides a
438 measure of the local variation between the radiation from flares and their immediate surroundings.
439 Across the Niger Delta flares are positioned in a variety of environmental contexts (mangrove
440 swamps, rainforest, offshore) with varying background radiance, therefore a given volume of com-
441 busted gas may lead to different total radiance emissions from the flare site depending on the con-
442 text. Therefore, incorporation of σr into the MOVET model provides the contextual information
443 that effectively normalises the total radiation from each flaring site by accounting for varying local
444 conditions.

445 

446

447 The predictive power of the MOVET model was tested using the leave-one-out cross valida-
448 tion method (Arlot and Celisse, 2010) based on the sample of 29 flare sites. This revealed a RMSE
449 of 0.007 Billion Cubic Metres (BCM) per month (28% of the mean), equating to an annual estima-
450 tion error of 0.084BCM for individual flare sites.

451 **3.4. Estimating volumetric rate of gas flaring in the Niger Delta (2000 – 2013)**

452 The MOVET was applied to each temporal composite MODIS band 22 image for January and
453 December of each sample year in order to estimate the volume of gas flared at all identified flare
454 sites. In order to estimate the annual total volume of gas flared at each site, we needed to derive es-
455 timates of flaring volume in each month of the year. We observed from the available summary of
456 monthly volumes reported for 2005 (the only year for which monthly data was available) that

457 monthly variation in flaring in the region was minimal with a coefficient of variation of 9.6% and
458 no systematic seasonal fluctuation. This indicated that it was acceptable to quantify monthly flaring
459 volumes based on the January and December estimates from MOVET. Therefore, for each flare site,
460 the volume estimates derived from the January and December monthly temporal composites in the
461 same calendar year were interpolated linearly to estimate volumes for all months of that year. The
462 twelve monthly volume estimates were then summed in order to calculate an annual volume of gas
463 combusted for each flare site. This process was repeated across the MODIS archive in order to de-
464 rive an annual estimate for volume of gas combusted at each flare site for each year from 2000 to
465 2013. The volume combusted at each site was summed over the entire study period and totals were
466 calculated for each state in the Niger Delta and the whole region. Uncertainty in the flare volume
467 estimates was expressed using the upper and lower 99% confidence intervals for the slope and in-
468 tercept derived from the calibration of the MOVET (see section 3.3) for individual flare sites, scaled
469 to annual estimates for states and the study site, as appropriate.

470

471 **4.0 Results**

472 *4.1 Spatial and temporal distribution of flare sites in the Niger Delta*

473 The MOVET detected 271 flare sites (190 onshore and 81 offshore) from 2000 to 2014. The
474 spatial distribution of the flares across the states of the Niger Delta is shown in Figure 6. The figure
475 also illustrates the number of times each of the flare sites was detected within the study period
476 based on an annual sampling interval, which is indicative of the duration of activity at each site. For
477 clarity, the number of detections recorded in Figure 6 do not represent detections in individual
478 MODIS images, rather they represent the number of detections in each of the bi-monthly temporal
479 composites from each sample year. This is why the maximum number of detections is 15, where an
480 individual flare has been detected in all of the 15 bi-monthly temporal composites that were ana-
481 lysed between 2000 and 2014.

482

483

Insert Figure 6 here

484 The number of flare sites identified per state is shown in Table 4. Rivers State had the highest
 485 proportion of flare sites in the region over the study period (27%), closely followed by Delta State
 486 (26%). Whilst Akwa Ibom State had only 13% of flares sites, it possessed the greatest proportion of
 487 offshore flare sites in the region, with 37% of all offshore flare sites in the Niger Delta being locat-
 488 ed in this state.

489 **Table 4.** Distribution of flare sites across the Niger Delta States (2000-2014)

State	Onshore flare sites	Offshore flare sites	All flare sites
Rivers	56	16	72
Delta	51	19	70
Bayelsa	41	12	53
Akwa Ibom	6	30	36
Edo	19	0	19
Ondo	5	4	9
Imo	11	0	11
Abia	1	0	1
Total	190	81	271

490 The temporal trajectory of flaring activity across the Niger Delta is shown in Figure 7, which
 491 indicates a downward trend from the peak in 2000 to 2014. Each sampling interval indicates a
 492 maintenance or decrease in flaring activity, with the largest decreases from 2000 to 2001 and 2013
 493 to 2014 with the only increase in activity from 2010 to 2011.

495 Insert Figure 7 here

496 **4.2 Spatial and temporal distribution of the volume of gas flared in the Niger Delta**

497 The outputs of the MOVET suggest that there was a wide variation in the annual volume of gas
 498 flared at individual flow stations (Table 5). This table shows the specific flare sites which have the
 499 smallest and largest volumes of gas combustion within each year, along with the annual mean and
 500 standard deviation. The maximum volume for an individual flare site was 4.60BCM, which was
 501 recorded in 2005 in Rivers State (MODET 58), and the minimum volume of 0.0363BCM was rec-
 502 orded in Imo State (MODET 224) in 2009. From the peak at 2005, there was a general reduction in
 503 the mean volume of gas combusted at individual flare sites and a decrease in the variability of flared
 504 volume.

505

506
507

Table 5. Summary of annual variations in volume of gas estimated for individual flare sites. The uncertainties are computed based on the upper and lower confidence 99% limits

Year	Min (BCM)	Uncertainty (±)	Flare ID	State	Location	Max (BCM)	Uncertainty (±)	Flare ID	State	Location	Mean (BCM)	Uncertainty (±)	Std DEV
2000	0.0370	0.013	MFDT 52	Rivers	Onshore	1.596	0.463	MFDT 58	Rivers	Onshore	0.192	0.057	0.256
2001	0.0369	0.012	MFDT 268	Edo	Onshore	2.383	0.691	MFDT 58	Rivers	Onshore	0.209	0.062	0.325
2002	0.0372	0.013	MFDT 339	Delta	Onshore	2.039	0.592	MFDT 58	Rivers	Onshore	0.200	0.060	0.296
2003	0.0369	0.012	MFDT 98	Rivers	Onshore	3.013	0.874	MFDT 58	Rivers	Onshore	0.221	0.066	0.350
2004	0.0364	0.012	MFDT 367	Bayelsa	Onshore	3.792	1.099	MFDT 58	Rivers	Onshore	0.225	0.067	0.414
2005	0.0374	0.013	MFDT 217	Rivers	Onshore	4.602	1.333	MFDT 58	Rivers	Onshore	0.265	0.078	0.501
2006	0.0372	0.013	MFDT 332	Edo	Onshore	3.606	1.045	MFDT 58	Rivers	Onshore	0.249	0.074	0.448
2007	0.0371	0.013	MFDT 339	Delta	Onshore	2.860	0.829	MFDT 61	Rivers	Onshore	0.249	0.074	0.416
2008	0.0372	0.013	MFDT 114	Ondo	Onshore	1.941	0.563	MFDT 22	Rivers	Onshore	0.192	0.057	0.314
2009	0.0363	0.012	MFDT 224	Imo	Onshore	1.022	0.297	MFDT 75	Rivers	Onshore	0.161	0.048	0.175
2010	0.0372	0.013	MFDT 2	Edo	Onshore	1.123	0.327	MFDT 75	Rivers	Onshore	0.142	0.043	0.167
2011	0.0373	0.013	MFDT 332	Edo	Offshore	2.043	0.593	MFDT 231	Akwa Ibom	Offshore	0.159	0.048	0.255
2012	0.0369	0.012	MFDT 106	Rivers	Onshore	2.253	0.654	MFDT 231	Akwa Ibom	Offshore	0.157	0.047	0.269
2013	0.0370	0.013	MFDT 227	Akwa Ibom	Offshore	0.475	0.139	MFDT 87	Rivers	Offshore	0.100	0.031	0.094

508
509
510
511
512
513
514
515
516
517
518
519
520
521
522

523 Figure 8 shows the spatial distribution of individual flare sites and the total volume of gas
524 combusted at each site over the study period. Figure 8 also shows the total volume of gas flared
525 within each state over the study period. The results demonstrate that the volume of gas flared at in-
526 dividual sites varied by over two orders of magnitude, as did the volume of gas flared across the
527 states. Rivers State flared the greatest volume of gas (135BCM) over the study period, followed by
528 Bayelsa State (71BCM). Figure 9 summarises variations in flaring activities between states in the
529 region over the study period. Most states showed an initial phase of increasing activity followed by
530 a general decrease, although the timing of these phases differs between states and some states do
531 not show this pattern of activity. Figure 9 also shows that there are wide variations between states in
532 the contributions of onshore and onshore flaring, and in those states where there is a mixture there
533 are differing trajectories of onshore and offshore activity with offshore generally becoming more
534 prevalent over time.

535 Insert Figure 8 here
536

537 Insert Figure 9 here
538

539 Figure 10 shows the trajectory of annual volumes of gas flared across the whole Niger Delta
540 region over the study period. This reveals that flaring activity increased initially, reaching a maxi-
541 mum (36BCM) in 2005 before subsequently declining from 2006 to 2009. There was however, a
542 brief increase in activity from 2010 to 2011, followed by another period of decline to the present
543 levels. These annual volume estimates derived from the MOVET show a reasonably close corre-
544 spondence with the trend of the reported volumes of gas flared for the Niger Delta published by the
545 NNPC (2012) (also shown in Figure 10). There are some discrepancies, notably at the middle of the
546 study period where the MOVET estimates showed much greater variability than the reported fig-
547 ures. Official reports are not available for 2013, but the MOVET indicated a substantial reduction in
548 flaring volume in the final stage of the study period. The MOVET outputs produced an estimate that
549 a total of 350 BCM of gas was flared in the region from March 2000 to January 2014.

550 Insert Figure 10 here
551

552 **5.0 Discussion**

553 The location of flare sites detected by the MODET varied considerably at the state level, with some
554 states such as Rivers and Delta having substantially more terrestrial flare sites than offshore, whilst
555 others such as Akwa Ibom had the inverse. However, the regional distribution of the flare sites
556 shows that there are more flare sites in the terrestrial environment than the marine environment.
557 This explicit level of variation detected using MODIS data is important as it may be used to isolate
558 and specifically study the varying impacts of flare sites for any particular area. For example flaring
559 in Akwa Ibom State is expected to have greater impact on the marine environment than the terres-
560 trial environment, based on the distribution of the flare sites shown in Figure 6. On the other hand,
561 the terrestrial environment of Rivers State will be the most impacted. Furthermore, the spatial dis-
562 tribution of the flares and the number of times they were detected over the study period showed var-
563 ious clusters of flaring activity. This suggests that the environmental impacts of flaring could be
564 highly heterogeneous, with extreme values in certain locations.

565 The MODET revealed an overall reduction in the number of active flare sites between 2000 and
566 2014 (Figure 5). This may have been as a result of the decommissioning of some flare sites due to
567 the commencement of full operations at the Nigerian Liquefied Natural Gas facility at Bonny Island
568 in late 1999 and subsequent commissioning of additional gas liquefaction trains from 2002, which
569 led to increased commercial utilisation of gases associated with extracted crude oil (NLNG, 2013).
570 The noticeable downward trend in the number of flare sites between 2006 and 2009 corresponds to
571 the period when oil and gas production in the region was severely disrupted by the Niger Delta mili-
572 tants (Paki and Ebiefa, 2011; Punch Newspaper, 2009). Also towards the end of 2005 gas plants
573 were commissioned at Kwale/Okpai by Nigeria Agip Oil Company, and Okoloma by the Shell Pe-
574 troleum Development Company (SPDC, 2011), both of which became fully operational from 2006.
575 The gas recycled from these plants is utilised in the generation of up to 1000MW of electric power

576 (National Petroleum Investment Management Services, 2010). The brief increase in numbers of
577 flare sites between 2010 and 2011, marked the return of relative peace in the region at the com-
578 mencement of the Amnesty programme by the Federal Government of Nigeria (BBC, 2009), which
579 appears to have enabled a short period of increased oil and gas production. Since 2011 there has
580 been a steady decline in the number of active flare sites through to present. During this period there
581 has not been any significant unrest in the region that could disrupt oil and gas production, hence the
582 decrease in numbers of flare suggests a decline in the use of flaring to dispose of gas. This may be a
583 consequence of the Soku liquefied natural gas feeder plant, which supplies 40% of the 22 million
584 tonnes of gas per annum (30BCM) to the liquefaction facility at Bonny Island, returning to full op-
585 eration towards the end of 2009 (Fineren, 2009). There has also been installation of associated gas
586 gathering infrastructure at various oilfields in the Niger Delta by the oil companies, such as those at
587 Forcados-Yokri and Southern Swamps (SPDC, 2013), which has reduced the requirement for flar-
588 ing. Hence, the results indicate that the oil and gas companies may finally be working towards the
589 eradication of gas flaring in the region. However, further monitoring of the situation using the
590 MODET is required in order to confirm this trend in subsequent years.

591 The MOVET showed that there was considerably variability between individual flare sites
592 in the volume of gas flared per annum and this is a reflection of the varying quantities of gas pro-
593 duced at the different flow stations. Gas produced at flow stations varies due to the commissioning
594 or decommissioning of oil wells that are feeding into a station, changes in the rate of oil and gas pro-
595 duction from individual wells and inter and intra well variation in the ratio of associated gas to oil
596 during the production cycle (International Association of Oil and Gas Producers, 2000). Interest-
597 ingly, the minimum volume combusted by an individual flare site was recorded in 2009 which coincid-
598 ed with the peak in social unrest in the region, which drastically disrupted oil production activities.
599 However, of greater significance is the systematic decrease in maximum and mean volumes com-
600 busted by individual flare sites since 2005 (Table 4). This suggests that in addition to the decrease
601 in the number of active flare sites (discussed above), for the remaining active sites, the rate of gas

602 combustion has also decreased which may be a result of reduced production from the wells contrib-
603 uting to flow stations and/or implementation of alternative strategies for dealing with associated
604 gas.

605 The state-level trajectories of the volumes of gas combusted (Figure 7) illustrated the specific
606 contributions of onshore and offshore flares to the total for each state as well as annual variations in
607 those contributions. We found that prior to the recent decline in flaring activity in 2013, in states
608 such as Rivers (which has the highest flaring volume among the states) and Akwa Ibom there was a
609 noticeable decline in onshore flaring volume, while the offshore volume gradually increased over
610 the same period. This suggests intensified offshore oil exploitation and decreasing onshore activities
611 in these states, which could be as a result of discoveries of new offshore oilfields such as Bonga,
612 Oyo, Ofon, Usan and Egina. Delta State however, shows a recent increase in onshore flaring vol-
613 ume after an initial decline and steadily decreasing offshore flaring activity. In addition there is a
614 general decline in onshore and offshore flaring volume in Bayelsa State. It was also found that alt-
615 hough Delta State had a greater number of active flare sites than Akwa Ibom or Bayelsa states,
616 greater volumes of gas were combusted in Akwa Ibom (71BCM over the study period) and Bayelsa
617 State (61BCM) than in Delta State (49BCM). This could be due to a lower gas to oil ratio in the oil-
618 fields in Delta State, or because a larger proportion of the gas produced from Delta State is being
619 utilized at recycling locations such as the Forcados-Yokri and Southern Swamp AGG, as well as the
620 Kwale/Okpai gas plant, which are all located in Delta State. As these observations demonstrate, a
621 significant advantage of the MOVET is the ability to provide information with sufficient spatial
622 precision to permit analysis of oil exploitation strategies in different states and, potentially, detailed
623 evaluation of the impacts of gas flaring. This level of information has not been previously explored
624 in flare-related research using remote sensing which has tended to focus on national or global scales
625 (Elvidge *et al.*, 2009a, 2009b, Casadio *et al.*, 2012), whereas the emphasis with MOVET is at the
626 level of the individual flow station.

627 The regional trajectory of the volume of gas combusted (Figure 8) showed a general increase
628 in the first half of the study period corresponding with increasing oil production, followed by a de-
629 crease in the second half in response to reduced oil production due to social disruption in the region,
630 in conjunction with the introduction of measures to reduce flaring such as liquefaction of gas. The
631 regional trajectory also indicated that the infrastructure for reducing gas flaring was already in place
632 by the end of the period of unrest in 2009, because although oil production returned to levels expe-
633 rienced before the period of unrest, the volume of gas flared continued to decrease. There is an
634 overall tendency for the estimates for gas flaring from MOVET to be higher than the reported val-
635 ues, with a notable discrepancy during the period of peak flaring in 2005-2006. This highlights the
636 importance of having an alternative means of obtaining information on gas flaring that is independ-
637 ent of official sources which rely on data provided by the oil companies. Our method determined
638 that a considerable volume of natural gas (350 BCM) has been flared in the region over the study
639 period; this has an energy value of 3.71×10^9 MWh which, by way of comparison, is approximately
640 10 times the annual electrical power consumption of the United Kingdom. Assuming that 184kg of
641 carbon dioxide is produced per MWh of natural gas (DEFRA, 2013), the gas flared in the Niger
642 Delta over the study period has resulted in 682.64Mt of carbon dioxide being released to the atmos-
643 phere, suggesting a significant contribution of greenhouse gasses and other pollutants during this
644 period.

645 Owing to the low spatial resolution of MODIS data, the spatial accuracy of the MODET was
646 found to be 844m, which is very much lower than the 24m spatial accuracy obtained from the Land-
647 sat Flare Detection Method (Anejionu *et al.*, 2014). However, for regional and state-based studies
648 such as that undertaken here, the MODET appears adequate. Indeed, the distribution of active flare
649 sites in the Niger Delta detected with MODIS data closely corresponds with that obtained from
650 Landsat (Anejionu *et al.*, 2014). The low spatial resolution of MODIS data may also have resulted
651 in the non detection of low intensity flares, leading to the under-detection of 9.3% based on the cal-
652 culated producer's accuracy of the MODET. Nevertheless, the spatial resolution of the data did not

653 restrict the user's accuracy. Cloud cover was a limiting factor encountered in the course of this re-
654 search. As with many areas of the world the Niger Delta is heavily cloud covered and this limits the
655 sampling opportunities for passive optical remote sensing. However, the frequent revisit times of
656 the Terra and Aqua platforms meant that it was possible to construct cloud-free temporal composite
657 images which formed the basis of the MODET and MOVET. The temporal sampling was limited to
658 certain months of the year and it was not possible to characterise intra-annual variations in gas flar-
659 ing activity, but the temporal sampling was sufficient for monitoring the longer-term inter-annual
660 trajectories in flaring. While the annual estimates of flaring volume from MOVET were based on
661 the reasonable assumption that intra-annual variations are minimal at active flare sites, it is likely
662 that estimates could be improved if more frequent sampling was possible. In this context, the com-
663 bination of information derived from MODIS together with that from other passive and active satel-
664 lite systems, may help to reduce the impacts of cloud cover and thereby increase the temporal sam-
665 pling opportunities. For instance, it has been shown that SOUMI VIIRS data is valuable for flare
666 detection (Elvidge *et al.*, 2013). Furthermore, pre-launch algorithm development has demonstrated
667 the potential of the forthcoming Sea and Land Surface Temperature Radiometer on Sentinel-3 in
668 gas flare detection (Wooster *et al.*, 2012). These systems are expected to play active role in the fu-
669 ture monitoring of gas flaring activities around the world.

670

671

672 **6.0 Conclusion**

673 This research has demonstrated the utility of MODIS data for detecting individual gas flare
674 sites and estimating the volume of gas combusted at these sites. Two MODIS-based techniques,
675 MODET and MOVET were developed which were capable of providing alternative sources of
676 information on gas flaring activity. The techniques were applied to the Niger Delta region and the
677 outputs provided detailed information on the spatial and temporal variability of gas flaring activity
678 in the region for the past 14 years.

679 The methods developed in this research provide an objective means of monitoring gas flar-
680 ing activity which is particularly important in areas such as the Niger Delta, where investigations of
681 gas flaring have previously been hampered by restricted access to official information on flares. Us-
682 ing freely-available MODIS data, the MODET and MOVET are consistent across different oil
683 fields; they are timely and reduce delays associated with traditional methods of acquiring flaring
684 data; and the data is independent of particular companies or authorities. In principle, with the
685 MODET and MOVET flaring can be investigated at spatial scales ranging from that of the individ-
686 ual flare site up to global level and across the time scale covered by the MODIS archive. However,
687 it is now important that the robustness and transferability of the techniques is evaluated in other oil-
688 producing regions of the world. This will enable the methods to make a key contribution to moni-
689 toring the compliance of countries to the Global Gas Flaring Reduction initiative and for modelling
690 the health and environmental impacts of flaring.

691

692 **Acknowledgements**

693 We wish to acknowledge the Surveyors Council of Nigeria (SURCON), who partly supported the
694 initial stages of this project with a research grant, the Department of Geoinformatics and Surveying,
695 University of Nigeria Enugu Campus, for the provision of the political map used in this research
696 and the Petroleum Technology Development Fund (PTDF Nigeria) who sustained the later stages of
697 this research via a scholarship. Thanks also to Lancaster University for the award of William Ritch-

698 ie Travel Grant, Lancaster Environment Centre and the Faculty of Science and Technology (Lan-
699 caster University) for the awards of travel grants for conferences. Gratitude to NASA for the
700 MODIS data used in the research.

701 **References**

- 702 Abdulkareem, A. S. (2005a). Evaluation of ground level concentration of pollutant due to gas flaring by
703 computer simulation: A case study of Niger - Delta area of Nigeria.
704 http://lejpt.academicdirect.org/A06/29_42.htm (accessed 14th November, 2013).
- 705 Abdulkareem, A.S. Afolabi, A.S. Abdulfatai, J., Uthman, H., & Odigure, J.O., (2012). Oil Exploration and
706 Climate Change: A case study of heat radiation from gas flaring in the Niger Delta area of Nigeria.
707 *InTech*, 1-27.
- 708 Arlot, S. & Celisse, A. (2010). A survey of cross-validation procedures for model selection. *Statistics Sur-*
709 *veys*, 4, 40–79.
- 710 Anomohanran, O. (2012). Thermal effect of gas flaring at Ebedei area of Delta State, Nigeria. *Pacific Jour-*
711 *nal of Science and Technology*, 13(2):555-560.
- 712 African Technology Policy Studies Network (ATPS). (2013). Multi-temporal threshold algorithm in forest
713 fire detection using MSG satellite: The case of Zimbabwe. *ATPS Working Paper No. 76*.
- 714 Anejionu C.D.O., Blackburn, G.A., & Whyatt, J.D. (2014). Satellite survey of gas flares: development and
715 application of a Landsat-based technique in the Niger Delta. *International Journal of Remote Sensing*,
716 35(5), 1900-1925.
- 717 BBC NEWS, 2009, Nigeria offers militants amnesty. <http://news.bbc.co.uk/1/hi/8118314.stm> (accessed on
718 17th April, 2012).
- 719 Casadio, S., Arino, O., & Serpe, D. (2012a). Gas flaring monitoring from space using the ATSR instrument
720 series. *Remote Sensing of Environment*, 116, 239–249.
- 721 Casadio, S., Arino, O., & Minchella, A. (2012b). Use of ATSR and SAR measurements for the monitoring
722 and characterisation of nighttime gas flaring from off-shore platforms: The North Sea test case. *Re-*
723 *remote Sensing of Environment*, 123, 175–186.
- 724 Casadio, S., & Arino, O. (2009). A new algorithm for the ATSR World Fire Atlas. *Proceedings EARSEL*
725 *2009 Symposium*. http://due.esrin.esa.int/wfa/Casadio_Arino_Earsel_2009.pdf. (accessed on 23rd July,
726 2012).
- 727 Casanova, J.L., Calle, A., Romo, A., & Sanz, J. (2005). Forest fire detection and monitoring by means of
728 an integrated MODIS-MSG system. *Remote Sensing Laboratory of University of Valladolid*.
729 http://www.iki.rssi.ru/earth/articles/sec9_12.pdf (accessed on 12th February, 2011)
- 730 Croft, T.A. 1978. Nighttime images of the earth from space. *Scientific American*, 239, 68-79.
- 731
- 732 Csiszar, I., Schroeder, W., Giglio, L., Justice, C.O., & Ellicott, E. (2012). Establishing active fire data conti-
733 nuity between Aqua MODIS and SUOMI NPP VIIRS.
734 [http://www.star.nesdis.noaa.gov/jpss/documents/meetings/2012/AMS_NewOrleans_2012/Oral/2012_](http://www.star.nesdis.noaa.gov/jpss/documents/meetings/2012/AMS_NewOrleans_2012/Oral/2012_AMS_Csiszar_Fire_V1.pdf)
735 [AMS_Csiszar_Fire_V1.pdf](http://www.star.nesdis.noaa.gov/jpss/documents/meetings/2012/AMS_NewOrleans_2012/Oral/2012_AMS_Csiszar_Fire_V1.pdf) (accessed on 3rd July, 2014).
- 736 Department of Environment Food and Rural Affairs (DEFRA) (2013). *2013 Government GHG Conversion*
737 *Factors for Company Reporting: Methodology Paper for Emission Factors*.
738 [https://www.gov.uk/government/uploads/system/uploads/attachment_data/file/224437/pb13988-](https://www.gov.uk/government/uploads/system/uploads/attachment_data/file/224437/pb13988-emission-factor-methodology-130719.pdf)
739 [emission-factor-methodology-130719.pdf](https://www.gov.uk/government/uploads/system/uploads/attachment_data/file/224437/pb13988-emission-factor-methodology-130719.pdf) (Accessed on 9th March, 2014).
- 740 Dozier, J. (1981). A method for satellite identification of surface temperature fields of subpixel resolution,
741 *Remote Sensing of Environment*, 11, 221-229.
- 742 Dung, E.J., Bombom, L.S., & Agusomu, T.D. (2008). The effects of gas flaring on crops in the Niger Delta,
743 Nigeria. *GeoJournal*, 73, 297–305.
- 744 Elvidge, C.D., Baugh, K.E., Tuttle, B.T., Howard, A.T., Pack, D.W., Milesi, C., & Erwin, E.H. (2007). A
745 twelve year record of national and global gas flaring volumes estimated using satellite data. *Final report*

746 to the World Bank. http://siteresources.worldbank.org/INTGGFR/Resources/DMSP_flares_
747 20070530_b-sm.pdf (accessed on 11th October, 2009).

748 Elvidge, C.D., Ziskin, D., Baugh, K.E., Tuttle, B.T., Ghosh, T., Pack, D.W., Erwin, E.H. & Zhizhin, M.
749 (2009a). A fifteen year record of global natural gas flaring derived from satellite data. *Energies*, 2,
750 595-622.

751 Elvidge, C.D., Baugh, K.E., Tuttle, B.T., Ziskin, D., Ghosh, T., Zhizhin, M., & Pack, D.W. (2009b). Improv-
752 ing satellite data estimation of gas flaring volumes. *Year two final report to the GGFR*.
753 http://www.ngdc.noaa.gov/dmsp/interest/flare_docs/NGDC_flaring_report_20090817.pdf. (accessed on
754 1st February 2011).

755 Elvidge, C.D., Baugh, K.E., Ziskin, D., Anderson, S., & Ghosh, T. (2011). Estimation of gas flaring volumes
756 using NASA MODIS Fire detection products. *Report presented to NASA*.

757 Elvidge, C.D., Zhizhin, M., Hsu, F., and Baugh, K.E. (2013). VIIRS Nightfire: Satellite Pyrometry at Night.
758 *Remote Sensing*, 5, 4423-4449.

759 Fineren, D. (2009). Nigeria LNG sees stable Soku gas feed by 2010-exec. *Reuters*.
760 <http://uk.reuters.com/article/2009/12/02/nigeria-lng-soku-idUSGEE5B11YU20091202> (Accessed on 9th
761 March, 2014).

762

763 Flasse, S.P., & Ceccato, P.S. (1996). A contextual algorithm for AVHRR fire detection. *International Jour-*
764 *nal of Remote Sensing* 17, 419 – 424.

765 Friends of the Earth. (2005). Communities sue Shell to stop Nigerian gas flaring. Archived press release.
766 http://www.foe.co.uk/resource/press_releases/communities_sue_shell_to_s_20062005.html (accessed
767 on 5th October, 2009).

768 Friends of the Earth. (2004). *Shell oil and gas flaring in Nigeria*.
769 http://www.foe.co.uk/resource/images/shell_nigeria_2006/slides/EG_Gas%20flare%20Kolo%20Creek%20shot%201.html (accessed on 5th October, 2009).

770

771 Gallegos, S., Ryan, R.E., Baud, R., & Bloemker, J.M. (2007). MODIS products to improve the monitoring of
772 gas flaring from offshore oil and gas facilities. *Final Report to NASA*.

773 Giglio, L., Descloitres, J., Justice, C.O., & Kaufman, Y.J. (2003). An enhanced contextual fire detection al-
774 gorithm for MODIS. *Remote Sensing of Environment* 8, 273–282.

775 Giglio, L., Schroeder, W., Boschetti, L., Roy, D., Justice, C. (2014). Collection 6 MODIS Fire Products.
776 Presented at MODIS Science Team Meeting at the Sheraton Columbia Town Center in Columbia, Mary-
777 land (April 29 - May 1).

778 Holben, B.N. (1986). Characteristics of maximum-value composite images from temporal AVHRR data. *In-*
779 *ternational Journal of Remote Sensing*, 7, 1417–1434.

780 Huete, A., Didan, K., Miura, T., Rodriguez, E., Gao, X., & Ferreira, L. (2002). Overview of the radiometric
781 and biophysical performance of the MODIS vegetation indices. *Remote Sensing of Environment*, 83,
782 195–213.

783 Ichoku, C., Kaufman, Y. J., Giglio, L., Li, Z. Fraser, R. H., Jin, J.Z., & Park, W. M. (2003). Comparative
784 analysis of daytime fire detection algorithms using AVHRR data for the 1995 fire season in Canada:
785 perspective for MODIS. *International Journal of Remote Sensing*, 24 (8), 1669–1690.

786 International Association of Oil and Gas Producers (OGP). (2000). Flaring and venting in the oil and gas ex-
787 ploration and production industry: An overview of purpose, quantities, issues, practices and trends.
788 *Report No. 2.79/288*.

789 Jonsson, P., & Eklundh, L. (2004). TIMESAT-a program for analyzing time-series of satellite sensor data.
790 *Computers Geosciences*, 30, 833-845.

791 Justice, C.O., Giglio, L., Korontzi, S., Owens, J., Morisette, J.T., Roy, D., Descloitres, J., Alleaume, S.,
792 Petitcoline, F., & Kaufman, Y. (2002). The MODIS fire products. *Remote Sensing of Environment* 83,
793 244 – 262.

794 Justice, C., Giglio, L., Boschetti, L., Roy, D., Csiszar, I., Morisette, J., & Kaufman, Y. (2006). Algorithm
795 Technical Background Document: MODIS Fire Products.
796 http://modis.gsfc.nasa.gov/data/atbd/atbd_mod14.pdf. (accessed on 10th March, 2011).

797 Kaufman, Y.J., Justice, C., Flynn, L., Kendall, J., Prins, E., Ward, D. E., Menzel, P., & Setzer, A. (1998).
798 Monitoring Global Fires from EOS-MODIS. *Journal of Geophysical Research*, 103, 32215-32338.

- 799 Lanorte, A., Danese, M., Lasaponara, R., & Murgante, B. (2011). Multiscale mapping of burn area and se-
800 verity using multisensor satellite data and spatial autocorrelation analysis. *International Journal of*
801 *Applied Earth Observation and Geoinformation xxx*, xxx–xxx
- 802 Li, Z., Kaufman, Y.J., Ichoku, C., Fraser, R., Trishchenko, A., Giglio, L., Jin, J., & Yu, X. (2000). A review
803 of AVHRR-based active fire detection algorithms: principles, limitations, and recommendations.
804 http://www.fao.org/gtos/gofc-gold/docs/fire_ov.pdf. (accessed on 4th February, 2011).
- 805 Martín. M. P., Flasse, S., Downey, I., & Ceccato, P. (1999). Fire detection and fire growth monitoring using
806 satellite data.
807 [http://publiclibrary.rfs.nsw.gov.au/CommonDocuments/7300FiredetectionMicrosoft%20Word%20-](http://publiclibrary.rfs.nsw.gov.au/CommonDocuments/7300FiredetectionMicrosoft%20Word%20-%20review.pdf)
808 [%20review.pdf](http://publiclibrary.rfs.nsw.gov.au/CommonDocuments/7300FiredetectionMicrosoft%20Word%20-%20review.pdf). (accessed on 10th March, 2011).
- 809 Matson, M. and Dozier, J. (1981). Identification of subresolution high temperature sources using a thermal
810 IR sensor. *Photogrammetric Engineering and Remote Sensing*, 47:1311.
- 811 MODIS Characterization Support Team. (2012). MODIS Level 1B In-Granule Calibration Code
812 (MOD_PR02) High-Level Design. *MCST Internal Memorandum # M1057 - REV. B*.
813 [http://mcst.gsfc.nasa.gov/sites/mcst.gsfc/files/file_attachments/M1057_High-](http://mcst.gsfc.nasa.gov/sites/mcst.gsfc/files/file_attachments/M1057_High-Level_Design_082212_REV_B_final_xg.pdf)
814 [Level_Design_082212_REV_B_final_xg.pdf](http://mcst.gsfc.nasa.gov/sites/mcst.gsfc/files/file_attachments/M1057_High-Level_Design_082212_REV_B_final_xg.pdf) (accessed on 2nd July, 2014).
- 815 Movaghati S., Samadzadegan F., & Azizi A. (2009). An Agent-Based Approach for Regional Forest Fire
816 Detection using MODIS Data. *Journal of Applied Sciences* 9 (20), 3672 - 3681.
- 817 Muirhead, K., & Cracknell, A.P. (1984). Identification of gas flares in the North Sea using satellite data. *In-*
818 *ternational Journal of Remote Sensing*, 5 (1), 199 - 212.
- 819 National Petroleum Investment Management Services (NAPIMS) (2010). NNPC/AGIP JV to commence 2nd
820 phase of Kwale-Okpai IPP soon.
821 [http://dev.nnpcgroup.com/napims/AboutUs/NAPIMSNews/tabid/245/articleType/ArticleView/articleI](http://dev.nnpcgroup.com/napims/AboutUs/NAPIMSNews/tabid/245/articleType/ArticleView/articleId/246/NNPCAGIP-JV-TO-COMMENCE-2ND-PHASE-OF-KWALE-OKPAI-IPP-SOON.aspx)
822 [d/246/NNPCAGIP-JV-TO-COMMENCE-2ND-PHASE-OF-KWALE-OKPAI-IPP-SOON.aspx](http://dev.nnpcgroup.com/napims/AboutUs/NAPIMSNews/tabid/245/articleType/ArticleView/articleId/246/NNPCAGIP-JV-TO-COMMENCE-2ND-PHASE-OF-KWALE-OKPAI-IPP-SOON.aspx). (Ac-
823 cessed on 9th, March, 2014).
- 824 National Population Commission (NPC). (2010). 2006 Population and Housing Census: population distribu-
825 tion by sex, state, LGA and senatorial district.
- 826 Nigerian Liquefied Natural Gas at Bonny Island – NLNG. (2013). Our Company: History.
827 <http://www.nlng.com/PageEngine.aspx?&id=44> (accessed on 24th October, 2013).
- 828 Nigeria National Petroleum Corporation - NNPC. (2010). Annual statistics bulletin. www.nnpcgroup.com .
829 accessed on 10th March, 2012).
- 830 Obia, A.E., Okon, H.E., Ekum, S.A., Eyo-Ita, E.E., & Ekpeni, E.A. (2011). The influence of gas flare partic-
831 ulates and rainfall on the corrosion of galvanized steel roofs in the Niger Delta, Nigeria. *Journal of*
832 *Environmental Protection*, 2, 1341-1346 doi:10.4236/jep.2011.210154.
- 833 Odjugo, P.A.O., & Osemwenkhae, E.J. (2009). Natural gas flaring affects microclimate and reduces maize
834 (*Zea mays*) yield. *International Journal of Agriculture and Biology*, 11: 408–412.
- 835 Onwuka, S. (2003). Nigeria: Shell builds locally fabricated flow station. *Daily Champion Newspaper* (29th
836 September, 2003).
- 837 Oseji, O.J. (2011). Environmental impact of gas flaring within Umutu-Ebedei gas plant in Delta State, Nige-
838 ria. *Archives of Applied Science Research*, 2011, 3 (6):272-279.
- 839 Ovri, J.E.O. Iroh, M. (2013). Corrosion Effect of Gas Flaring On Galvanized Roofing Sheet in Imo State,
840 Nigeria. *The International Journal of Engineering and Science*, 2 (1), 339-345.
- 841
- 842 Ovuakporaye, S.I., Aloamaka, C.P., Ojieh, A.E., Ejebe, D.E. & Mordi, J.C. (2012). Effect of Gas Flaring on
843 Lung Function among Residents in Gas Flaring Community in Delta State, Nigeria. *Research Journal*
844 *of Environmental and Earth Sciences*, 4(5), 525-528.
- 845 Paki, F.A.E., & Ebienna, K. I. (2011). Militant Oil Agitations in Nigeria’s Niger Delta and the Economy. *In-*
846 *ternational Journal of Humanities and Social Science*, 1 (5), 140-145.
- 847 Prins, E.M., & Menzel, W.P. (1992). Geostationary satellite detection of biomass burning in South America.
848 *International Journal of Remote Sensing*, 13 (15), 2783-2799.
- 849 Punch Nigerian Newspaper. (2009). Upsurge of Militancy in Niger Delta.
850 <http://archive.punchng.com/Articl.aspx?theartic=Art20090303762220>. (accessed on 20th October,
851 2011).
- 852 Qian, Y., Yan, G., Duan, S., & Kong, S. (2009). A Contextual Fire Detection Algorithm for Simulated HJ-
853 1B Imagery. *Sensors*, 9, 961-979.

- 854 Roberts, G. Wooster, M. J., Perry, G. L. W., Drake, N., Rebelo, L.M., and Dipotso, F. (2005). Retrieval of
855 biomass combustion rates and totals from fire radiative power observations: Application to southern Af-
856 rica using geostationary SEVIRI imagery. *Journal of Geophysical Research*, 110 (D21111), 1 - 19.
- 857 Roberts, G.J., & Wooster, M.J. (2008). Fire detection and fire characterization over Africa using Meteosat
858 SEVIRI. *IEEE Transactions on Geoscience And Remote Sensing*, 46 (4), 1200 - 1218.
- 859 Royal Geography Society. (2013). Spearman's rank correlation coefficient–Excel guide
860 <http://www.rgs.org/NR/rdonlyres/4844E3ABB36D4B148A203A3C28FAC087/0/OASpearmanRank>
861 [ExcelGuidePDF.pdf](#) (accessed on 15th July, 2013)
- 862 Sedano, F., Kempeneers, P., San Miguel, J., Strobl, P., & Vogt, P. (2013). Towards a pan European burnt scar
863 mapping methodology based on single date medium resolution optical remote sensing data. *Interna-
864 tional Journal of Applied Earth Observation and Geoinformation*, 20, 52-59.
- 865 Shell Petroleum Development Company of Nigeria (SPDC) (2013). Shell in Nigeria: Gas flaring.
866 [http://s02.static-shell.com/content/dam/shell-new/local/country/nga/downloads/pdf/2013bnotes/gas-
867 flaring.pdf](http://s02.static-shell.com/content/dam/shell-new/local/country/nga/downloads/pdf/2013bnotes/gas-flaring.pdf) (accessed on 9th March, 2014).
- 868 Shell Petroleum Development Company of Nigeria (SPDC) (2011). Shell in Nigeria: The Afam VI Power
869 Generating Plant and Okoloma NAG Facility. [http://s00.staticshell.com/content/dam/shell-
870 new/local/country/nga/downloads/pdf/2013bnotes/afam.pdf](http://s00.staticshell.com/content/dam/shell-new/local/country/nga/downloads/pdf/2013bnotes/afam.pdf) (accessed on 9th, March, 2014).
- 871 Smith, A.M.S., Wooster, M.J. 2005. Remote classification of head and backfire types from MODIS fire radi-
872 ative power and smoke plume observation. *International Journal of Wildland Fire*, 14, 249 -254
- 873 Stoms, D.M., Bueno, M.J., & Davis, F.W. 1997. Viewing geometry of AVHRR image composites derived
874 using multiple criteria. *Photogrammetric Engineering & Remote Sensing*, 63, 6, 681-689.
- 875 Wang, S.D., Miaoa, L.L., & Peng, G.X. (2012). An improved algorithm for forest fire detection using HJ
876 data. *Procedia Environmental Sciences*, 13, 140 – 150.
- 877 Weaver, J. F., Lindsey, D. T., Bikos, D. E., Schmidt, C. C., & Prins, E. 2004. *Fire detection using GOES-11
878 rapid scan imagery*. *Weather and Forecasting*, 19, 496-510.
- 879 Wooster, M.J., Zhukov, B., Oertel, D. (2003). Fire radiative energy for quantitative study of biomass burn-
880 ing: derivation from the BIRD experimental satellite and comparison to MODIS fire products. *Remote
881 Sensing of Environment*, 86, 83-107.
- 882 Wooster, M.J., Xu, W., & Nightingale, T. (2012). Sentinel-3 SLSTR active fire detection and FRP product:
883 Pre-launch algorithm development and performance evaluation using MODIS and ASTER datasets.
884 *Remote Sensing of Environment*, 120, 236–254.
- 885 Xu, W., Wooster, M. J., Roberts, G., & Freeborn, P. (2010). New GOES imager algorithms for cloud and
886 active fire detection and fire radiative power assessment across North South and Central America. *Re-
887 mote Sensing of Environment*, 114, 1876–1895.
- 888 Zhukov, B., Lorenz, E., Oertel, D., Wooster, M.J, & Roberts, G. (2006). Spaceborne detection and charac-
889 terization of fires during the bi-spectral infrared detection (BIRD) experimental small satellite mission
890 (2001–2004). *Remote Sensing of Environment*, 100, 29-51.

List of Figure captions

- 891
- 892
- 893
- 894
- 895 **Figure 1.** Map of the Niger Delta region, showing its component oil producing states. Map of Nigeria is inset.
- 896
- 897 **Figure 2.** Spectral band images demonstrating the gas flare detection potential of day time and nighttime MODIS band
898 22 and daytime band 7 (band 6 showed a very similar response). Bands 6 and 7 are turned off at nighttime.
- 899
- 900 **Figure 3.** Flow chart illustrating the key stages of the MODIS Flare Detection Technique (MODET), based on the har-
901 nessing of radiometric and spatial properties of flares in nighttime band 22 imagery.
- 902
- 903 **Figure 4.** An active flare in the Agbada oilfield (Rivers State) of the Niger Delta captured in a high resolution image on
904 Google Earth
- 905
- 906 **Figure 5.** Scatterplot of the radiance of flare sites (quantified by the product of the square of the sum of radiance and
907 standard deviation of radiance values in the buffer zone around flare pixels) and recorded volume of gas flared at sam-
908 ple flow stations in the Niger Delta, used for calibrating the MOVET model.
- 909

910 **Figure 6.** Map showing the spatial distribution of flare sites identified in the Niger Delta with the MODIS Flare Detection Technique from March 2000 to January 2014. Flare sites detected once are those that are newly detected in 2013/14.

911
912
913 **Figure 7.** Flare sites detected in the Niger Delta from 2000 to 2014. The positive error bar (9.3%) is based on the producer's accuracy of the MODET while absence of a negative error bar reflects the 100% user's accuracy.

914
915
916 **Figure 8.** The distribution of volume of gas combusted at individual flare sites (represented by the size of the symbol that shows the location of each site) and within each state (represented by the colour shading of each state) over the study period (2000-2014).

917
918
919
920 **Figure 9.** Trajectories of annual gas flaring volume (BCM) within the individual states in the Niger Delta over the study period, indicating the contribution of onshore (blue bars) and offshore (red bars) flaring towards each annual total.

921
922
923 **Figure 10.** Graph showing the temporal trajectory of annual flaring volume estimated using the method developed in this research compared to reported annual volumes and annual crude oil production within the study area. Error bars represent the 99% confidence interval derived from the calibration of the MOVET.

924
925
926
927